

Charge Transfer Complexes of the Donor Acriflavine and the Acceptors Quinol, Picric acid, TCNQ and DDQ: Synthesis, Spectroscopic Characterizations and Antimicrobial Studies

Hala H. Eldaroti^{1,*}, Suad A. Gadir¹, Moamen S. Refat^{2,3} and Abdel Majid A. Adam²

¹ Chemistry Department, Faculty of Education, Alzaeim Alazhari University, Khartoum, Sudan

² Chemistry Department, Faculty of Science, Taif University, 888 Taif, Saudi Arabia

³ Chemistry Department, Faculty of Science, Port Said University, Egypt

*E-mail: halahassan_1972@yahoo.com

Received: 18 February 2013 / Accepted: 13 March 2013 / Published: 1 April 2013

Four new charge-transfer (CT) complexes have been formed in the reaction of the topical antiseptic agent acriflavine (Acf) with the acceptors quinol (QL), picric acid (PA), tetracyanoquinodimethane (TCNQ) and dichlorodicyanobenzoquinone (DDQ). The reactions have been studied spectrophotometrically in methanol and the formed solid complexes were isolated and characterized through elemental analysis, electronic absorption, spectrophotometric titration, IR, Raman, ¹H-NMR and X-ray powder diffraction (XRD) techniques as well as thermal analysis and scanning electron microscopy (SEM). The reaction stoichiometries, donor: acceptor molar ratio values, were found to be 1:2 ratio for QL and PA complexes and 1:1 ratio for TCNQ and DDQ complexes. Accordingly the formed CT complexes could be formulated as [(Acf)(QL)₂], [(Acf)(PA)₂], [(Acf)(TCNQ)] and [(Acf)(DDQ)]. Finally, the CT complexes were screened for their antibacterial and antifungal activities against various bacterial and fungal strains, and the complex obtained using QL acceptor exhibited good antimicrobial activities against all of the tested strains compared with standard drugs.

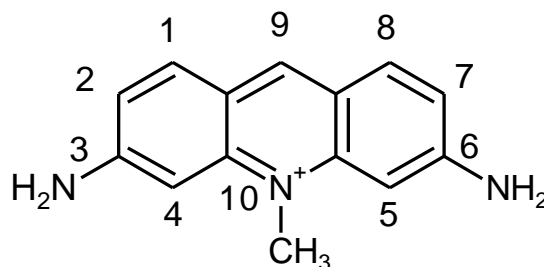
Keywords: Acriflavine, Charge-transfer, XRD, SEM, thermal analysis, Biological activity.

1. INTRODUCTION

Acriflavine (Acf; 3,6-diamino-10-methylacridinium chloride) (Formula I) also called Acriflavinium chloride, is a kind of topical antiseptic agent derived from acridine, first synthesized in 1912 by Paul Ehrlich, a German medical researcher and was used in the early 20th century, during the First World War, as topical antibacterial and against sleeping sickness [1-4]. Acriflavine is

widely used for photosensitizer [5], analytical reagents for sensing [6], acid-base indicator [7], luminescence sensors [8], among many others. Acriflavine has proved an effective agent for gonorrhea, meningitis, intestinal infections, diphtheria, pneumonia, cholera and infected wounds; in some countries is at present formulated with urotropine as well known urinary tract antiseptic [9]. In recent years, acriflavine has also been used in AIDS treatments. Thus, the acriflavine-AZT (azido-deoxythymidine)-ellipticine combination is reportedly the most appropriated and efficient treatment for eradication of HIV1 infections [9].

In this paper herein, we report the formation of new CT complexes obtained in the reaction of Acf with the electron acceptors quinol (QL), picric acid (PA), tetracyanoquinodimethane (TCNQ) and dichlorodicyanobenzoquinone (DDQ) using methanol as a solvent. The newly synthesized CT complexes have been structurally characterized via elemental analysis; infrared (IR), Raman, $^1\text{H-NMR}$ and electronic absorption spectroscopy; powder X-ray diffraction; and scanning electron microscopy (SEM) to interpret the behavior of the interactions. The thermal behavior of the obtained complexes and the kinetic and thermodynamic parameters have also been investigated. Finally, the antimicrobial activity of the Acf CT complexes was tested against various bacterial and fungal strains.



Formula I. Chemical structure of Acriflavine.

2. EXPERIMENTAL

2.1 Reagents

Acriflavine (Acf; 3,6-diamino-10-methylacridin-10-ium chloride, $\text{C}_{14}\text{H}_{14}\text{ClN}_3$) and π -acceptors of quinol (QL), picric acid (PA), 7,7',8,8'-tetracyanoquinodimethane (TCNQ) or 2,3-dichloro-5,6-dicyano-1,4-benzoquinone (DDQ) were obtained from Merck Chemical Company and were used without further purification. Commercially available spectroscopic grade solvents (BDH) were also used as purchased.

2.2 Synthesis of the solid CT-complexes

The solid CT complexes of Acf with QL, PA, TCNQ or DDQ were synthesized by mixing 1 mmol Acf with 2 mmol of each acceptor in methanol (10 ml). The mixtures were stirred

at room temperature for 20 min, which resulted in the precipitation of the solid CT complexes. The solid precipitates were filtered, washed several times with methanol, and then dried under vacuum over anhydrous calcium chloride.

2.3 Photometric titration measurements

Spectrophotometric titration measurements were performed for the reactions of Acf with QL, PA, TCNQ or DDQ against methanol as a blank, at wavelengths of 300, 400, 300 and 285 nm, respectively. A 0.25, 0.50, 0.75, 1.00, 1.50, 2.0, 2.50, 3.00, 3.50 or 4.00 mL aliquot of a standard solution (5.0×10^{-4} M) of the appropriate acceptor in MeOH was added to 1.00 ml of 5.0×10^{-4} M Acf, which was also dissolved in MeOH. The total volume of the mixture was 5 mL. The concentration of Acf (C_d) in the reaction mixture was maintained at 5.0×10^{-4} M, whereas the concentration of the acceptors (C_a) changed over a wide range of concentrations (0.25×10^{-4} M to 4.00×10^{-4} M) to produce solutions with an acceptor molar ratio that varied from 4:1 to 1:4. The stoichiometry of the molecular CT complexes was obtained from the determination of the conventional spectrophotometric molar ratio according to known methods [10] using a plot of the absorbance of each CT complex as a function of the $C_d:C_a$ ratio. Modified Benesi–Hildebrand plots were constructed [11, 12] to allow the calculation of the formation constant, K_{CT} , and the absorptivity, ϵ_{CT} , values for each CT complex in this study.

2.4 Instrumental analyses

2.4.1 Elemental analyses

The elemental analyses of the carbon and hydrogen contents were performed by the microanalysis facility at Cairo University, Egypt, using a Perkin-Elmer CHN 2400 (USA).

2.4.2 Electronic spectra

The electronic absorption spectra of methanolic solutions of the donor, acceptors and resulting CT complexes were recorded over a wavelength range of 200–800 nm using a Perkin-Elmer Lambda 25 UV/Vis double-beam spectrophotometer at Taif University, Saudi Arabia. The instrument was equipped with a quartz cell with a 1.0 cm path length.

2.4.3 Infrared and Raman spectra

The mid-infrared (IR) spectra (KBr discs) within the range of $4000\text{--}400\text{ cm}^{-1}$ for the solid CT complexes were recorded on a Shimadzu FT-IR spectrophotometer with 30 scans at 2 cm^{-1} resolution. The Raman laser spectra of the samples were measured on a Bruker FT-Raman spectrophotometer equipped with a 50 mW laser at Taif University, Saudi Arabia.

2.4.4 $^1\text{H-NMR}$ spectra

$^1\text{H-NMR}$ spectra were collected by the Analytical Center at King Abdul Aziz University, Saudi Arabia, on a Bruker DRX-250 spectrometer operating at 250.13 MHz with a dual 5 mm probe head. The measurements were performed at ambient temperature using DMSO- d_6 (dimethylsulfoxide, d_6) as a solvent and TMS (tetramethylsilane) as an internal reference. The $^1\text{H-NMR}$ data are expressed in parts per million (ppm) and are internally referenced to the residual proton impurity in the DMSO solvent.

2.4.5 Thermal analysis

Thermogravimetric analysis (TGA) was performed under an air atmosphere between room temperature and 800 °C at a heating rate of 10 °C/min using a Shimadzu TGA-50H thermal analyzer at the Central Lab at Ain Shams University, Egypt.

2.4.6 X-ray diffraction patterns

The X-ray diffraction patterns for the obtained CT complexes were collected on a PANalytical X'Pert PRO X-ray powder diffractometer at the Central Lab at Ain Shams University, Egypt. The instrument was equipped with a Ge (III) monochromator, and a Cu $K\alpha_1$ X-ray source with a wavelength of 0.154056 nm was used.

2.4.7 SEM and EDX detection

Scanning electron microscopy (SEM) images were collected on a Jeol JSM-6390 instrument at Taif University, Saudi Arabia. The instrument was operated at an accelerating voltage of 20 kV.

2.5 Biological assessment

2.5.1 Antibacterial activity

The antimicrobial activities of the newly synthesized Acf CT complexes and the pure solvent were tested *in vitro* against two Gram-positive bacteria, *Staphylococcus aureus* (MSSA 22) and *Bacillus subtilis* (ATCC 6051), and two Gram-negative bacteria, *Escherichia coli* (K 12) and *Pseudomonas aeruginosa* (MTCC 2488), using a modified Bauer–Kirby disc diffusion method [13]. The microanalysis facility at Cairo University, Egypt performed the investigations. For these investigations, 100 μl test bacteria were grown in 10 ml fresh medium until they reached a count of approximately 10^8 cells/ml for bacteria or 10^5 cells/ml for fungi [14]. Then, 100 μl microbial suspension was spread onto agar plates. The nutrient agar medium for the antibacterial tests consisted of 0.5% peptone, 0.1% beef extract, 0.2% yeast extract, 0.5% NaCl and 1.5% agar-agar

[15]. Isolated colonies of each strain were selected from the primary agar plates and tested for susceptibility. After the plates were incubated for 48 h at 37 °C, the inhibition (sterile) zone diameters (including the disc) were measured using slipping calipers from the National Committee for Clinical Laboratory Standards (NCCLS, 1993) [16] and are expressed in mm. The screening was performed using 100 µg/ml CT complex. An antibiotic disc of tetracycline (30 µg/disc, Hi-Media) was used as a positive control.

2.5.2 Antifungal activity

The newly synthesized complexes were also screened for their antifungal properties against *Aspergillus flavus* (laboratory isolate) and *Candida albicans* (IQA-109) in DMSO using a modified Bauer–Kirby disc diffusion method [13]. The complex was dissolved in DMSO. The medium for the antifungal tests consisted of 3% sucrose, 0.3% NaNO₃, 0.1% K₂HPO₄, 0.05% KCl, 0.001% FeSO₄ and 2% agar- agar [15]. The disc diffusion method for the filamentous fungi was tested using the M38-A standard method [17], whereas the disc diffusion method for yeast was tested using the M44-P standard method [18]. Plates inoculated with filamentous fungi or yeast were incubated for 48 h at 25 °C or 30 °C, respectively. The antifungal activity of the CT complexes was compared with that of amphotericin B (30 µg/disc, Hi-Media) as a standard antifungal agent. Antifungal activity was determined by measuring the diameters of the sterile zone (mm) in triplicate.

3. RESULTS AND DISCUSSION

3.1 Elemental analysis results

Table 1. Elemental analyses and physical parameters data of the Acf CT-complexes.

Complex	MF	Mwt g/mol	Elemental analyses			
			C%		H%	
			Found	Calc.	Found	Calc.
[(Acf)(QL) ₂]	C ₂₆ H ₂₆ ClN ₃ O ₄	479.95	65.19	65.01	5.34	5.42
[(Acf)(PA) ₂]	C ₂₆ H ₁₈ ClN ₉ O ₁₄	717.93	43.07	43.46	2.62	2.51
[(Acf)(TCNQ)]	C ₂₆ H ₁₈ ClN ₇	463.92	66.89	67.25	3.80	3.88
[(Acf)(DDQ)]	C ₂₂ H ₁₄ Cl ₃ N ₅ O ₂	486.73	53.91	54.24	2.76	2.88

Elemental analyses (C and H) of the Acf CT complexes were performed, and the obtained analytical data along with some of the physical properties are listed in Table 1. From this table, it can be seen that the resulting values are in good agreement with the calculated values, and the suggested values are in agreement with the molar ratios determined from the photometric titration curves. The stoichiometry of the complexes were found to be 1:2 ratio for QL and PA complexes

and 1:1 ratio for TCNQ and DDQ complexes. All the complexes are insoluble in cold and hot water, but easily soluble in DMF and DMSO solvents.

3.2 Determination of stoichiometry of the resulting CT complexes

The electronic absorption spectra of the formed Acf CT complexes are shown in Fig. 1. These spectra revealed new absorption bands that are attributed to the CT interactions. These bands are observed at 300, 400, 300 and 285 for the [(Acf)(QL)₂], [(Acf)(PA)₂], [(Acf)(TCNQ)] and [(Acf)(DDQ)] complexes, respectively. These peak absorbance values that appeared in the spectra assigned to the formed CT complexes were measured and plotted as a function of the $C_d:C_a$ ratio according to a known method. Spectrophotometric titration plots based on these measurements are shown in Fig. 2. The stoichiometry ratio of the complex formation, (Acf: acceptor) was found to be 1:2 ratio for QL and PA complexes and 1:1 ratio for TCNQ and DDQ complexes. Based on the obtained data, the formed charge-transfer complexes were formulated as [(Acf)(QL)₂], [(Acf)(PA)₂], [(Acf)(TCNQ)] and [(Acf)(DDQ)]. These results are strongly supported by the elemental analyses.

3.3 Determination of formation constant (K_{CT}) and molar extinction coefficient (ϵ_{CT})

The spectrophotometric titrations of the intermolecular charge-transfer complexes formed from the reactions of Acf with QL and PA acceptors indicated the formation of 1:2 CT complexes; therefore, the formation constant (K_{CT}) and the molar absorptivity (ϵ) of these complexes were calculated by applying the 1:2 modified Benesi-Hildebrand equation in Eq. (1):

$$(C_a)^2 C_d/A = 1/K\epsilon + 1/\epsilon C_a (4C_d + C_a) \quad (1)$$

where C_a and C_d are the initial concentrations of the acceptor and the donor, respectively, and A is the absorbance of the strongly detected CT band. When the $(C_a)^2 C_d/A$ values for the 1:2 charge-transfer complex are plotted against the corresponding $C_a (4C_d + C_a)$ values, a straight line is obtained with a slope of $1/\epsilon$ and an intercept of $1/K\epsilon$. The obtained K_{CT} and ϵ values associated with the complexes are given in Table 2. The 1:1 Benesi-Hildebrand Eq. (2), was used to calculate the values of the formation constant and the molar absorptivity for the complexes of Acf with TCNQ and DDQ acceptors.

$$(C_a C_d)/A = 1/K\epsilon + (C_a + C_d)/\epsilon \quad (2)$$

where C_a and C_d are the initial concentrations of the acceptor and the donor, respectively, and A is the absorbance of the strongly detected CT band. When the $(C_a C_d)/A$ values for the 1:1 charge-transfer complex are plotted against the corresponding $(C_a + C_d)$ values, a straight line is obtained with a slope of $1/\epsilon$ and an intercept of $1/K\epsilon$. The values of both K_{CT} and ϵ associated

with the complexes are given in Table 2.

The K_{CT} and ϵ_{CT} values obtained throughout these calculations are given in Table 2. As expected, 1:2 Acf complexes (QL and PA) exhibit very high values for the formation constant (K_{CT}) than 1:1 complexes (TCNQ and DDQ), which reflect the high stabilities of the $[(Acf)(QL)_2]$ and $[(Acf)(PA)_2]$ complexes.

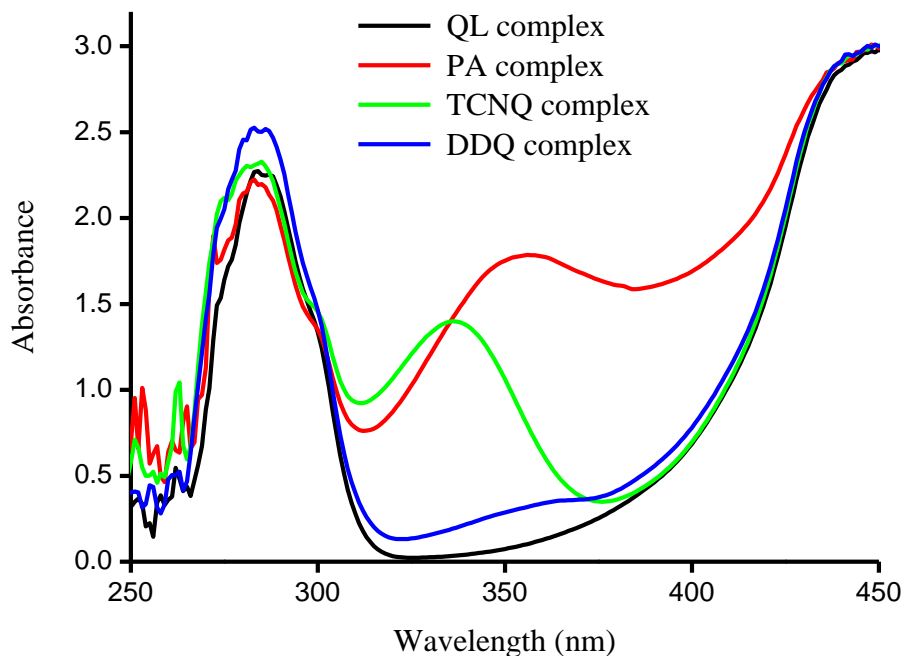
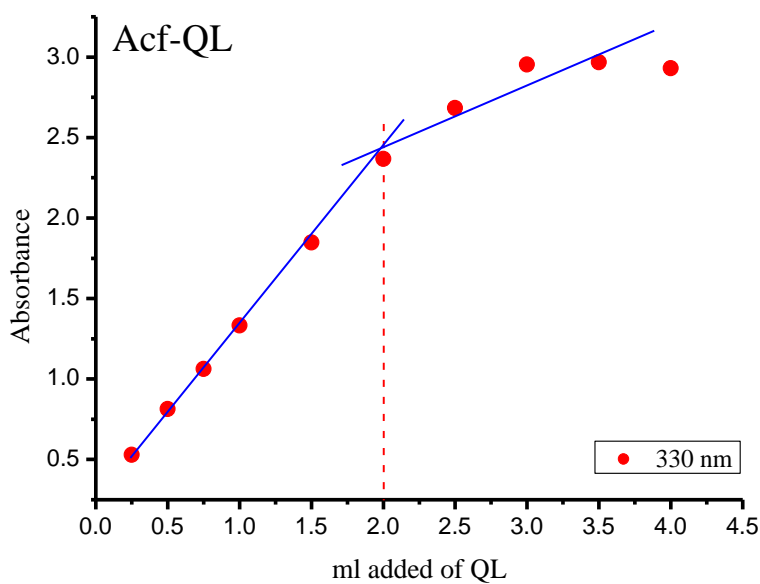


Figure 1. Electronic absorption spectra of Acf CT-complexes.



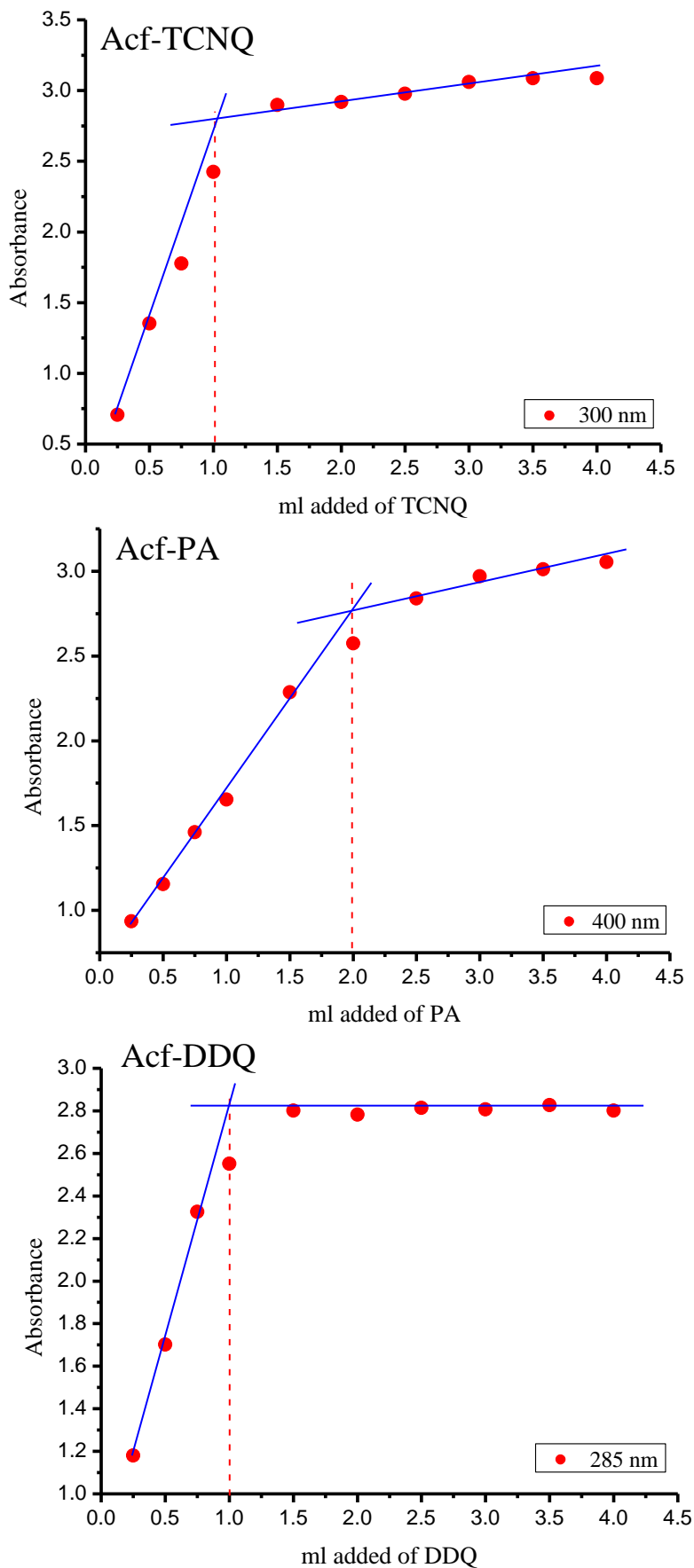


Figure 2. Photometric titration curve for Acf-QL, Acf-PA, Acf-TCNQ and Acf-DDQ systems at the detectable peaks.

The data also reveal that the [(Acf)(QL)₂] complex shows a higher K_{CT} value compared with the other complexes. This value is about twice times higher than the value of formation constant for the [(Acf)(PA)₂] complex. The value of formation constant of [(Acf)(TCNQ)] is higher than that of [(Acf)(DDQ)] (about four times higher), and this can be understood on the basis of the differences in the electronic structure of TCNQ and DDQ. The TCNQ acceptor has four strong withdrawing cyano groups in conjugation with an aromatic ring which causes high delocalization leads to a great increase in the Lewis acidity of the acceptor TCNQ, and hence the higher value of K_{CT} for [(Acf)(TCNQ)] complex compared with that of [(Acf)(DDQ)] complex.

3.4 Determination of the spectroscopic and physical data

The spectroscopic and physical data, such as the standard free energy (ΔG°), the oscillator strength (f), the transition dipole moment (μ), the resonance energy (R_N), and the ionization potential (I_p), were estimated for samples dissolved in methanol at

25 °C. The calculations can be summarized as follows.

3.4.1 Determination of oscillator strength (f)

From the CT absorption spectra, the oscillator strength (f) can be estimated using the approximate formula [19]:

$$f = 4.319 \times 10^{-9} \int \epsilon_{CT} d\nu \quad (3)$$

where $\int \epsilon_{CT} d\nu$ is the area under the curve of the extinction coefficient of the absorption band in question plotted as a function of frequency. To a first approximation,

$$f = 4.319 \times 10^{-9} \epsilon_{CT} \nu_{1/2} \quad (4)$$

where ϵ_{CT} is the maximum extinction coefficient of the CT band and $\nu_{1/2}$ is the half-bandwidth in cm^{-1} (i.e., the bandwidth at half of the maximum extinction coefficient value).

3.4.2 Determination of transition dipole moment (μ)

The transition dipole moments (μ) of the complexes have been calculated from Eq. (5) [20]:

$$\mu = 0.0958 [\epsilon_{CT} \nu_{1/2} / \nu_{max}]^{1/2} \quad (5)$$

The transition dipole moment can be used to determine if a particular transition is allowed; the transition from a bonding π orbital to an antibonding π^* orbital is allowed because the integral that defines the transition dipole moment is nonzero.

3.4.3 Determination of ionization potential (I_P) of the donor

The ionization potentials (I_P) of the Acf donor in the complexes were calculated using the empirical equation derived by Aloisi and Pignataro represented in Eq. (6) [21]:

$$I_P \text{ (eV)} = 5.76 + 1.53 \times 10^{-4} \nu_{CT} \quad (6)$$

where ν_{CT} is the wavenumber in cm^{-1} that corresponds to the CT band formed from the interaction between the donor and the acceptor. The electron-donating power of a donor molecule is measured by its ionization potential, which is the energy required to remove an electron from the highest occupied molecular orbital.

3.4.4 Determination of resonance energy (R_N)

Briegleb and Czekalla [22] theoretically derived the following relationship to obtain the resonance energy (R_N):

$$\varepsilon_{CT} = 7.7 \times 10^{-4} / [h\nu_{CT} / [R_N] - 3.5] \quad (7)$$

Where ε_{CT} is the molar absorptivity coefficient of the CT complex at the maximum of the CT absorption, ν_{CT} is the frequency of the CT peak, and R_N is the resonance energy of the complex in the ground state, which contributes to the stability constant of the complex (a ground-state property).

3.4.5 Determination of energy of the charge-transfer complex (E_{CT})

The energy values (E_{CT}) of the $n \rightarrow \pi^*$ and $\pi - \pi^*$ interactions between the donor (Acf) and the acceptors were calculated using the equation derived by Briegleb [23]:

$$E_{CT} = (h\nu_{CT}) = (1243.667 / \lambda_{CT}) \quad (8)$$

where λ_{CT} is the wavelength of the CT band.

3.4.6 Determination of standard free energy changes (ΔG°)

The standard free energy of complexation (ΔG°) for each complex was calculated from the formation constants using the equation [24]:

$$\Delta G^\circ = -2.303RT \log K_{CT} \quad (9)$$

where ΔG° is the free energy of the CT complexes (kJ mol^{-1}), R is the gas constant ($8.314 \text{ J mol}^{-1} \text{ K}^{-1}$), T is the absolute temperature in K, and K_{CT} is the formation constant of the complex (L mol^{-1}) at room temperature.

The calculated spectroscopic and physical values (f , μ , I_p , R_N and ΔG°) for the Acf CT complexes using these equations are presented in Table 2. The $[(\text{Acf})(\text{QL})_2]$ complex exhibits considerably higher values of both the oscillator strength (f) and the transition dipole moment (μ) compared to the other complexes. These high f values indicate a strong interaction between the donor–acceptor pairs with relatively high probabilities of CT transitions [25]. Among the numerous applications of CT complexes, one important application is the calculation of the ionization potential (I_p) of the donor. The calculated I_p value for the highest filled molecular orbital that participates in the CT interaction of the Acf donor is approximately 10.7. The ionization potential of the electron donor has been reported to be correlated with the charge-transfer transition energy of the complex [26]. Further evidence for the nature of the CT interactions is the calculation of the standard free energy change (ΔG°). The obtained values of ΔG° for the $[(\text{Acf})(\text{QL})_2]$, $[(\text{Acf})(\text{PA})_2]$, $[(\text{Acf})(\text{TCNQ})]$ and $[(\text{Acf})(\text{DDQ})]$ are -46, -45, -38 and -35 kJ mol^{-1} , respectively; these values indicate that the interaction between the Acf donor and the acceptors is spontaneous.

Table 2. Spectrophotometric data of the Acf CT-complexes.

Complex	λ_{max} (nm)	E_{CT} (eV)	K (Lmol^{-1})	ϵ_{max} ($\text{Lmol}^{-1}\text{cm}^{-1}$)	f	μ	I_p	R_N	ΔG° (kJ mol^{-1})
$[(\text{Acf})(\text{QL})_2]$	300	4.15	11.70×10^7	6.08×10^4	75.05	69.17	10.86	0.87	-46,034
$[(\text{Acf})(\text{PA})_2]$	400	3.11	6.37×10^7	6.10×10^4	27.73	48.55	9.59	0.65	-44,528
$[(\text{Acf})(\text{TCNQ})]$	300	4,15	5.16×10^4	3.86×10^4	41.68	51.55	10.86	1.18	-38,302
$[(\text{Acf})(\text{DDQ})]$	285	4.36	1.39×10^4	3.07×10^4	36.80	47.21	11.13	1.24	-35,039

3.5 IR and Raman spectra

Table 3. Assignments of the characteristic IR and Raman spectral bands (cm^{-1}) for Acf CT-complexes.

Complex	$\nu(\text{NH})$		$\delta(\text{NH}_3^+)_{\text{def}}$		$\delta(\text{NH}_3^+)_{\text{sym}}$		$\rho(\text{NH}_3^+)$		$\nu(\text{CN})$	
	IR	Raman	IR	Raman	IR	Raman	IR	Raman	IR	Raman
$[(\text{Acf})(\text{QL})_2]$	3218	3060	1644	1620	1360	1368	829	839	-	-
$[(\text{Acf})(\text{PA})_2]$	3224	3094	1610	1607	1320	1339	828	823	-	-
$[(\text{Acf})(\text{TCNQ})]$	-	-	-	-	-	-	-	-	2221	2224
$[(\text{Acf})(\text{DDQ})]$	-	-	-	-	-	-	-	-	2209	2223

The donation process from Acf donor to the acceptors can occur either from the lone pair of electron on the nitrogen atom of amino groups or from the aromatic rings. The nitrogen atoms have been identified as the donation source in most cases studied. The IR spectroscopy have been used to distinguish between the two possibilities. The peak assignments for the important characteristic IR

and Raman spectral bands for the formed Acf CT complexes are shown in Table 3, whereas the full IR spectra of the CT complexes are shown in Fig. 3.

In the IR spectra of the [(Acf)(QL)₂] and [(Acf)(PA)₂] complexes, the characteristic bands of Acf observed at 3300 and 3155 cm⁻¹, which are assigned to -NH₂ asymmetric and symmetric stretching vibrations, respectively [27], shifted and reduced in intensity after complexation. This observation clearly indicates that the -NH₂ group in the Acf donor participates in the complexation process. IR and Raman spectra confirm the presence of the main characteristic absorption bands that result from the stretching and bending deformation of the NH₃⁺ group. These bands; the ν(NH), ν_{def}(NH₃⁺), δ_{sym}(NH₃⁺) and ρ(NH₃⁺) absorptions are observed for [(Acf)(QL)₂] and [(Acf)(PA)₂] at approximately 3200, 1600, 1300 and 800 cm⁻¹, respectively (Table 3). The presence of these bands indicated that the complexation occurs through the protonation of the -NH₂ group of the Acf donor via a proton-transfer phenomenon from the acidic center of each acceptor to form NH₃⁺ ammonium based on acid-base theory [28-34]. In the IR spectra of the [(Acf)(TCNQ)] and [(Acf)(DDQ)] complexes, the following observations are recorded:

1- The absence of a few bands at approximately 2600-2400 cm⁻¹ due to the hydrogen bonding in the spectra of these complexes.

2- The band that results from the ν(C≡N) vibration of the free TCNQ and DDQ acceptors changed in frequencies and decrease in intensities in the complexes upon CT-complexation. Free TCNQ shows one ν(C≡N) vibration at 2220 cm⁻¹, while in its complex, ν(C≡N) occurs at lower wavenumber values, 2100 cm⁻¹. In free DDQ, ν(C≡N) occurs at 2231 and 2250 cm⁻¹, while in the complex it moved to 2209 cm⁻¹.

3- Generally, there are small changes in wavenumber values and intensities of the free reactants (Acf, TCNQ and DDQ) upon complexation. These changes and shifts in positions of some of the peaks could be understood on the basis of the expected symmetry and electronic structure modifications in both donor and acceptor units in the formed complex compared to the free molecules.

All these observations clearly indicate that the -NH₂ group in the Acf donor and the -C≡N group in the TCNQ or DDQ acceptors participated in the complexation process. Because TCNQ and DDQ lacks acidic centers, the molecular complexes can be concluded to form through π→π* and/or n→π* charge migration from the HOMO of the donor to the LUMO of the acceptor. The π→π* CT complex is formed via the benzene ring (electron-rich group) of the Acf and the TCNQ or DDQ reagents (electron acceptor) [35, 36]. The cyano group (-C≡N) is an electron-withdrawing group that exists in TCNQ and DDQ in a conjugated bonding system. The CN groups in TCNQ and DDQ withdraw electrons from the aromatic ring, and such a process will make the aromatic ring an electron-accepting region. The π*-CN electron density appears to increase and more easily accept a proton from the donor because of the electron-withdrawing process and the conjugated electron system. So, the interactions mode between Acf and the TCNQ and DDQ acceptors occur through the migration of a H⁺ ion to one of the cyano groups in the acceptors to form a positive ion (-C≡N H) that associates with the anion to form ion pairs [34, 37, 38].

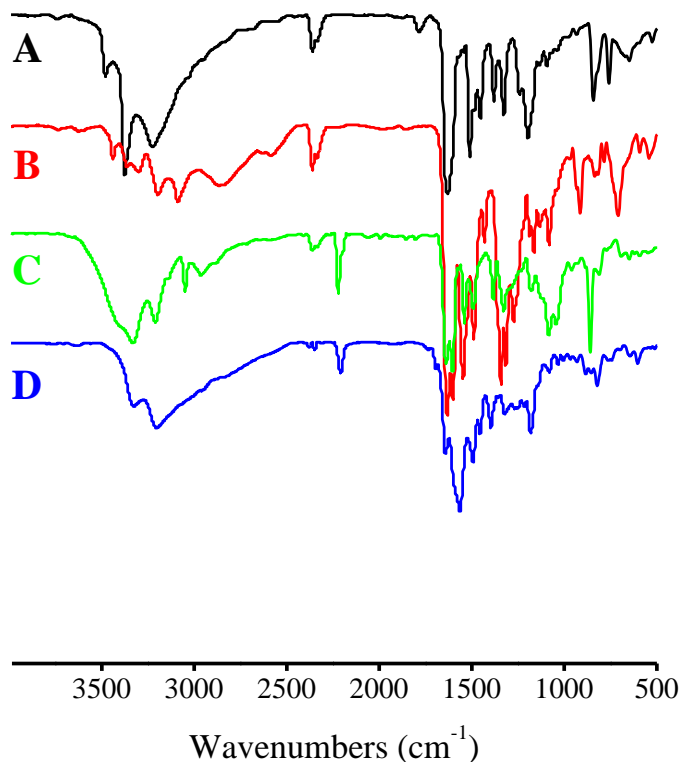
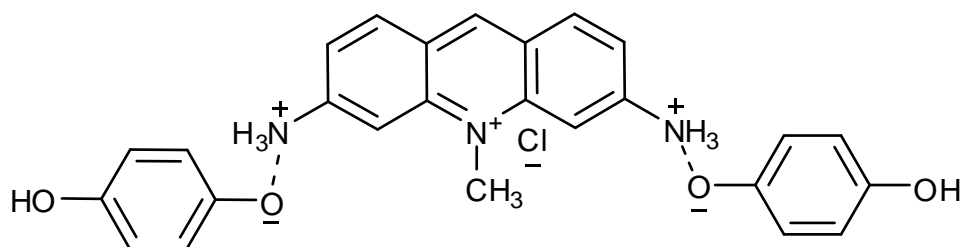


Figure 3. Infrared spectra of (A) Acf/QL, (B) Acf/PA, (C) Acf/TCNQ and (D) Acf/DDQ CT complexes.

3.6 $^1\text{H-NMR}$ spectra

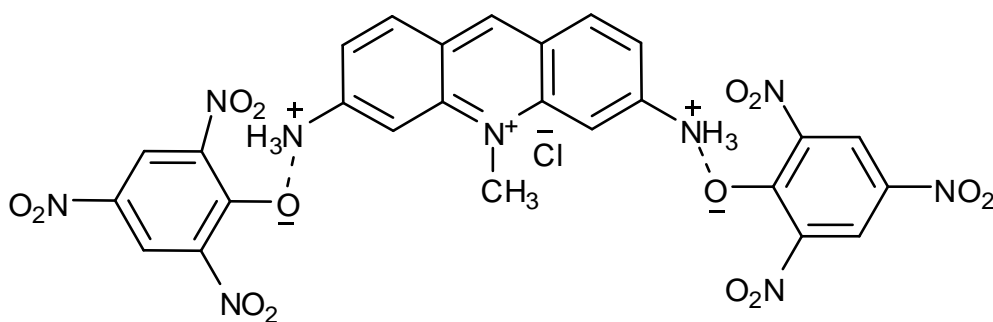
The 400 MHz $^1\text{H-NMR}$ spectra of the complexes were measured in $\text{DMSO-}d_6$ at room temperature and are given in Fig. 4. The chemical shifts (δ) of the different types of protons of the CT complexes are given below. The results obtained from the elemental analyses, infrared spectra, and photometric titrations are in agreement with the $^1\text{H-NMR}$ spectra, which allows for an interpretation of the mode of interaction between the donor and the acceptor. The reaction of Acf as the donor with QL as the acceptor yielded a new charge-transfer complex, (3,6-diammonio-10-methylacridinium bis (4-hydroxy-phenolate)) chloride, which produced signals at (Fig. 4): $\delta = 2.50$ (s, 3H, CH_3), 6.57 (s, 6H, 2NH_3^+), 6.96 (d, 2H, $J = 13.2$, Ar-H, $\text{C}_2\text{-H}$ and $\text{C}_6\text{-H}$ phenol), 7.01 (d, 2H, $J = 11.4$, Ar-H, $\text{C}_3\text{-H}$ and $\text{C}_5\text{-H}$ phenol), 7.51 (s, 2H, Ar-H, $\text{C}_4\text{-H}$, $\text{C}_5\text{-H}$ acridinium), 7.76 (d, 2H, $J = 12.6$, Ar-H, $\text{C}_2\text{-H}$, $\text{C}_7\text{-H}$ acridinium), 7.81 (d, 2H, $J = 12.0$, Ar-H, $\text{C}_1\text{-H}$, $\text{C}_8\text{-H}$ acridinium), 8.19 (s, 1H, Ar-H, $\text{C}_9\text{-H}$ acridinium), 8.68 (s, 2H, Ar-OH, phenolic OH). The $^1\text{H-NMR}$ spectrum of this complex indicated that the phenolic proton ($-\text{OH}$) signal, which is observed at approximately 8.59 ppm in the spectrum of the QL acceptor, decreased in intensity with a downfield shift for the non-hydrogen-bonded one (8.68 ppm) in the spectrum of the CT complex. This result indicates the involvement of one phenolic group in chelating through the deprotonation from the QL acceptor to the Acf donor. In addition, the disappearance of the $-\text{NH}_2$ protons from Acf and the appearance of a weak broad band at 6.57 ppm, which is attributed to the ammonium protons, indicate the involvement of the $-\text{NH}_2$ group in the complexation process. The aromatic protons of the

Acf which lie in the range of 7.51- 8.19 ppm showed no significant variation in the complex indicating non participation of the aromatic rings in the complex formation Based on these data, the structure suggested for the $[(\text{Acf})(\text{QL})_2]$ complex is shown in Formula II.



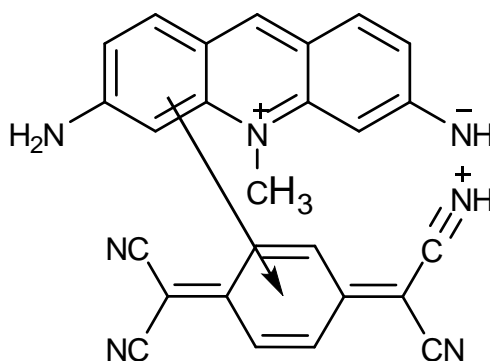
Formula II. Suggested structure of $[(\text{Acf})(\text{QL})_2]$ complex.

The $^1\text{H-NMR}$ spectrum for the CT complex formed with Acf and PA is shown in Fig. 4 and is summarized as follows: $\delta = 2.50$ (s, 3H, CH_3), 4.03 (b, 6H, 2NH_3^+), 7.30 (s, 2H, Ar-H, $\text{C}_4\text{-H}$, $\text{C}_5\text{-H}$ acridinium), 7.77 (d, 2H, $J = 12.6$, Ar-H, $\text{C}_2\text{-H}$, $\text{C}_7\text{-H}$ acridinium), 7.81 (d, 2H, $J = 12.0$, Ar-H, $\text{C}_1\text{-H}$, $\text{C}_8\text{-H}$ acridinium), 8.57 (s, 4H, Ar-H, picric acid proton), 8.73 (s, 1H, Ar-H, $\text{C}_9\text{-H}$ acridinium). In the charge-transfer reaction between Acf and PA, the proton of the -OH group of PA is transferred to the $-\text{NH}_2$ group of Acf to form an ion-paired compound named 3,6-diammonio-10- methylacridinium chloride bis (2,4,6-trinitrobenzenolate). The data obtained from $^1\text{H-NMR}$ spectrum of $[(\text{Acf})(\text{PA})_2]$ complex are in agreement with the suggested complexation assume that the amino group and phenolic group are mainly involved in the formation of the CT complex. The new peak observed at 4.03 ppm in the complex, which is not detected in the spectrum of the free donor, is attributed to the formation of a hydrogen bond [39] between PA and Acf. The peak at $\delta = 11.94$ ppm, which is assigned to the $-\text{OH}$ proton of the free picric acid acceptor [40], was absent in the spectrum of this complex, which is attributed to the formation of the CT complex. Together, these data indicate that the amino and phenolic groups are involved in the formation of the CT complex between Acf and PA. The characteristic signals presences within the range of 7.30-8.73 ppm were assigned to the protons of aromatic rings. Suggested structure for the $[(\text{Acf})(\text{PA})_2]$ complex is illustrated in Formula III.



Formula III. Suggested structure of $[(\text{Acf})(\text{PA})_2]$ complex.

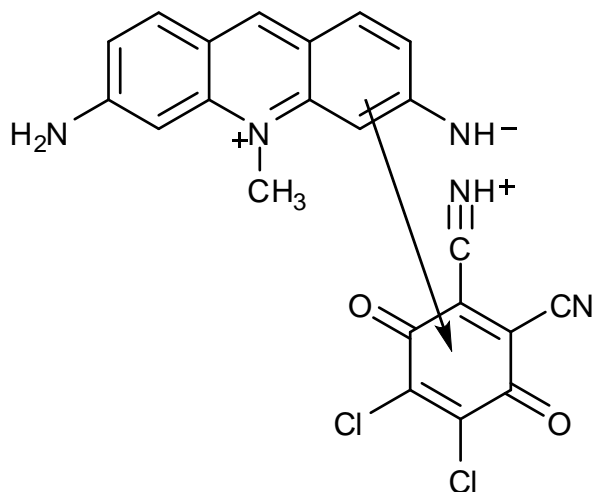
The $^1\text{H-NMR}$ spectrum for the CT complex between Acf and TCNQ is shown in Fig. 4 and is summarized as follows: $\delta = 2.50$ (s, 3H, CH_3), 3.21 (s, 2H, $\text{C}_6\text{-NH}_2$), 3.61 (s, 1H, NH^-), 6.37 (s, 1H, $\text{C}_5\text{-H}$, acridinium), 6.73 (s, 1H, $\text{C}\equiv\text{NH}^+$), 6.87 (d, 1H, $J = 13.8$ Hz, Ar-H, $\text{C}_7\text{-H}$ acridinium), 7.02 (d, 1H, $J = 13.8$ Hz, Ar-H, $\text{C}_8\text{-H}$ acridinium), 7.79 (d, 1H, $J = 13.2$ Hz, Ar-H, $\text{C}_2\text{-H}$ acridinium), 7.85 (d, 1H, $J = 12.6$, Ar-H, $\text{C}_1\text{-H}$ acridinium), 8.08 (s, 1H, Ar-H, $\text{C}_4\text{-H}$ acridinium), 8.74 (s, 1H, Ar-H, $\text{C}_9\text{-H}$ acridinium), 9.03 (s, 4H, Ar-H, TCNQ protons). In the charge-transfer reaction between Acf and TCNQ, the proton of the $-\text{NH}_2$ group in Acf is transferred to a nitrogen atom of TCNQ to form an ion-paired compound, specifically (2-cyano-2-(4-(dicyanomethylene) cyclohexa-2,5-dienylidene) ethylidene) ammonium (6-amino-10-methyl-acridinium-3-yl) amide chloride. The mode of chelation concerning $[(\text{Acf})(\text{TCNQ})]$ complex was sustained by the presence of two new signals at 6.73 and 3.61 ppm, which are assigned to the protons of (NH^+) and (NH^-) , respectively. These signals are not detected in the spectrum of the free donor, which indicates that the $-\text{NH}_2$ and $-\text{C}\equiv\text{N}$ groups are primarily involved in the formation of the CT complex between Acf and TCNQ. The migration of the H^+ ion from the NH_2 in the donor to one of the four cyano groups in the TCNQ acceptor resulted in the formation of a positive ion ($-\text{C}\equiv\text{N H}^+$), which is associated with the anion NH^- ; this result is also confirmed from the disappearance of the $-\text{NH}_2$ signal in the spectrum of Acf. According to these observations, the suggested structure of $[(\text{Acf})(\text{TCNQ})_2]$ complex is given in Formula IV.



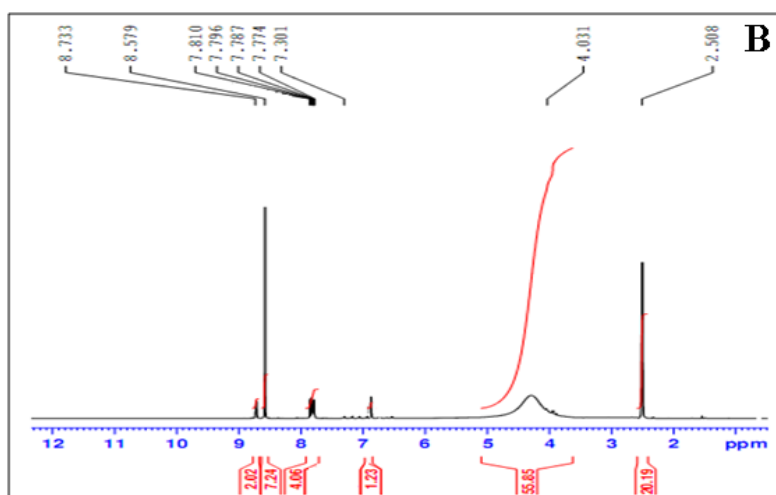
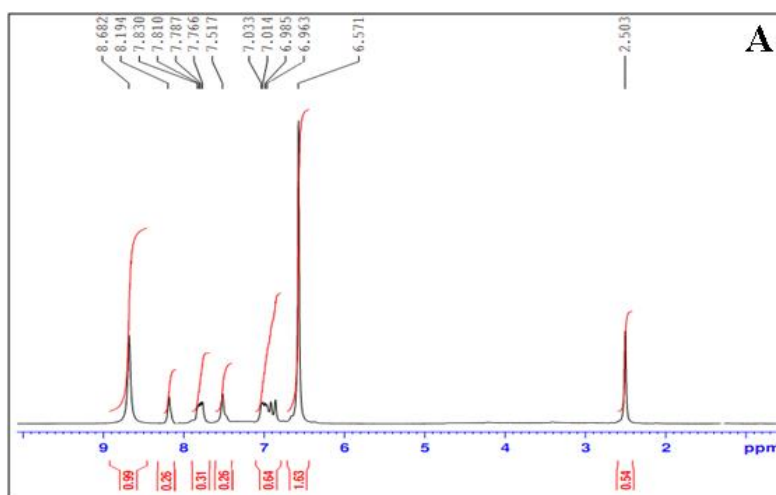
Formula IV. Suggested structure of $[(\text{Acf})(\text{TCNQ})]$ complex.

The reaction between Acf and DDQ afforded bis (((4,5-dichloro-2-cyano-3,6-dioxocyclohexa-1,4-dienyl) methylidene) ammonium)((6-amino-10-methylacridinium-3-yl) amide) chloride. $^1\text{H-NMR}$ spectrum for this compound is shown in Fig. 4 and is summarized as follows: $\delta = 2.50$ (s, 3H, CH_3), 3.39 (s, 2H, $\text{C}_6\text{-NH}_2$), 3.85 (b, 1H, NH^-), 6.62 (s, 1H, $\text{C}_5\text{-H}$, acridinium), 6.96 (s, 1H, $\text{C}\equiv\text{NH}^+$), 7.79 (d, 1H, $J = 13.8$ Hz, Ar-H, $\text{C}_7\text{-H}$ acridinium), 7.84 (d, 1H, $J = 13.8$ Hz, Ar-H, $\text{C}_8\text{-H}$ acridinium), 7.96 (d, 1H, $J = 13.2$ Hz, Ar-H, $\text{C}_2\text{-H}$ acridinium), 8.00 (d, 1H, $J = 12.6$, Ar-H, $\text{C}_1\text{-H}$ acridinium), 8.11 (s, 1H, Ar-H, $\text{C}_4\text{-H}$ acridinium), 8.72 (s, 1H, Ar-H, $\text{C}_9\text{-H}$ acridinium). The formation of the complex was confirmed by the appearance of two new signals observed at 6.96 and 3.85 ppm in the spectrum of the complex; which are attributed to the protons of (NH^+) and (NH^-) , respectively. These peaks are not detected in the spectrum of the free donor, which indicates that

the $-NH_2$ and $-C\equiv N$ groups are primarily involved in the formation of the CT complex. The suggested structure of [(Acf)(DDQ)] complex is given in Formula V.



Formula V. Suggested structure of [(Acf)(DDQ)] complex.



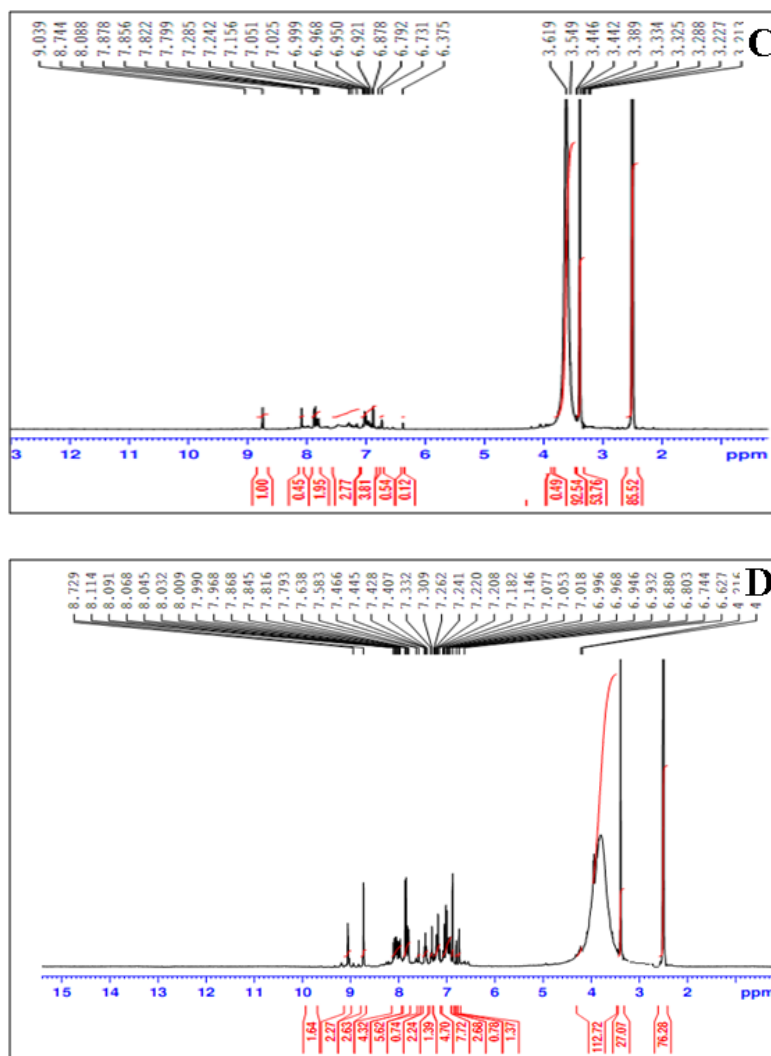


Figure 4. $^1\text{H-NMR}$ spectrum of (A) Acf/QL, (B) Acf/PA, (C) Acf/TCNQ and (D) Acf/DDQ.

3.7 Thermal analysis

To examine the thermal stability of the new complexes, the thermogravimetric analysis of the complexes were carried out over the temperature range of 25-800 °C under an air atmosphere. The TG curves were redrawn as mass loss versus temperature. Typical TG curves of the complexes are presented in Fig. 5, and the thermoanalytical results are listed in Table 4. The TG curve of [(Acf)(QL)₂] complex exhibited mass loss in three decomposition process between 25-370, 370-460 and 460-800 °C temperature range. The first decomposition step (obs. = 29.05, calc. = 29.27%) is attributed to the liberation of HCl, 2NH₃, C₂H₂ and CO₂ molecules. The second decomposition step (obs. = 30.10%, calc. = 29.59%) is reasonably explained by the loss of 4C₂H₂, NO₂ and 2CO₂ molecules. The third decomposition step existed within the temperature range 460-800, which is reasonably by the loss of C₂H₂, CO₂ and 3.5H₂ molecules. The three decomposition steps which has been assigned to the loss of HCl, 2NH₃, 6C₂H₂, NO₂, 4CO₂ and 3.5H₂ giving an overall mass loss of 75.97%, with a few carbon atoms remains as a final residual.

Table 4. Thermo analytical results for the Acf CT-complexes.

Complex	Stage	TG temp. range (°C)	Weight loss (%)		Evolved moiety
			Found	Calc.	
[(Acf)(QL) ₂] C ₂₆ H ₂₆ ClN ₃ O ₄	I	25-370	29.05	29.27	HCl+2NH ₃ +C ₂ H ₂ +CO ₂
	II	370-460	30.10	29.59	4C ₂ H ₂ +NO ₂ +2CO ₂
	III	460-800	16.83	16.04	C ₂ H ₂ +CO ₂ +3.5H ₂
	Residue	-	24.03	25.00	Residual carbon
[(Acf)(PA) ₂] C ₂₆ H ₁₈ ClN ₉ O ₁₄	I	25-285	27.77	27.93	HCl+2NH ₃ +C ₂ H ₂ +2NO ₂ +CO ₂
	II	285-490	25.83	25.77	NH ₃ +3C ₂ H ₂ +NO ₂ +CO ₂
	III	490-800	34.13	34.27	3NO ₂ +9CO ₂
	Residue	-	12.27	11.70	Residual carbon
[(Acf)(TCNQ)] C ₂₆ H ₁₈ ClN ₇	I	25-186	22.83	23.17	HCl+2HCN+NH ₃
	II	186-376	46.78	46.99	2HCN+5C ₂ H ₂ +2NO ₂ +0.5CO ₂
	II	376-800	14.40	14.23	5.5CO ₂
	Residue	-	15.99	15.52	Residual carbon
[(Acf)(DDQ)] C ₂₂ H ₁₄ Cl ₃ N ₅ O ₂	I	25-800	88.90	87.68	HCl+2Cl ₂ +NH ₃ +2HCN+4C ₂ H ₂ +2NO ₂ +7CO ₂
	Residue	-	11.10	12.32	Residual carbon

The thermogram of the [(Acf)(PA)₂] complex shows three main degradation steps between 25-285, 285-490 and 490-800°C temperature range, are associated with weight losses of 27.77, 25.83 and 34.13%, respectively, in addition to a carbon residue to 12.27%. The first decomposition step found within the temperature range 25-285 °C, corresponds to the loss of HCl, 2NH₃, C₂H₂, 2NO₂ and CO₂ molecules, with a weight loss of 27.77% very close to the expected theoretical value of 27.93%. The second decomposition step within the temperature range 285-490 °C, may be attributed to the liberation of NH₃, 3C₂H₂, NO₂ and CO₂ molecules with a weight loss of 25.83%. The final degradation step is associated with the loss of 3NO₂ and 9CO₂ molecules, with remaining few carbon atoms in the final step as a final residual. The [(Acf)(TCNQ)] complex decomposes in three definite decomposition steps within the 25-800 °C temperature range. The first decomposition step within the temperature range 25-186 °C corresponding to loss of HCl, 2HCN and NH₃ molecules representing a weight loss of (obs.= 22.83%, calc.= 23.17%). This step is followed by another degradation step corresponds to the liberation of 2HCN, 5C₂H₂, 2NO₂ and 0.5CO₂ molecules with a total weight loss of 46.78% with about 0.21% deviation from the calculated value (46.99%). After losing of 5.5CO₂ molecules in the final degradation step, a few carbon atoms are remaining as a final residue. The thermal decomposition of the [(Acf)(DDQ)] complex is a one- step process within the range of 200-800 °C, which is attributed to the loss of [C₂₂H₁₄Cl₃N₅O₂] as HCl, 2Cl₂, NH₃, 2HCN, 4C₂H₂, 2NO₂ and 7CO₂ molecules. This step is associated with a total weight loss of 88.9% which is in agreement with the calculated value (87.68%).

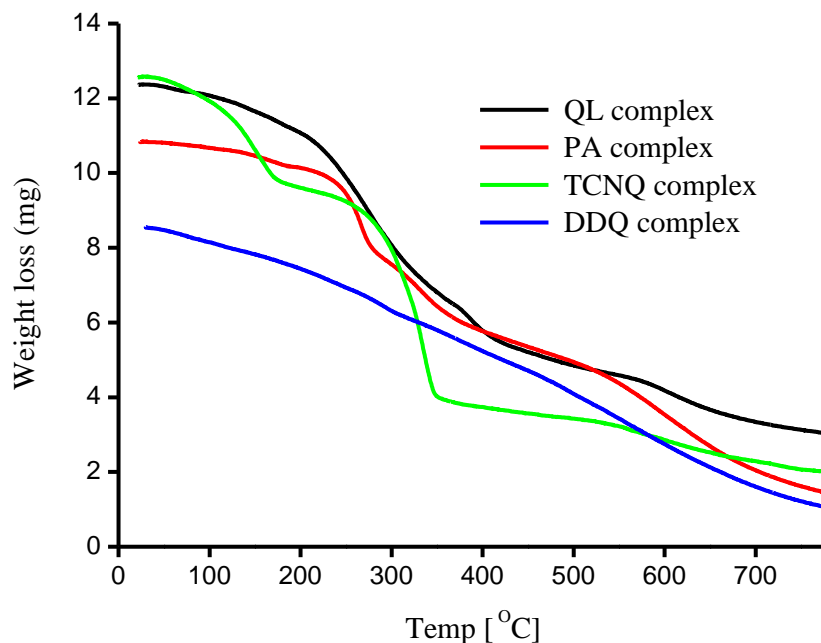


Figure 5. TG curves of Acf CT-complexes.

3.8 Kinetic and thermodynamic studies

Kinetic studies on thermal processes are expected to provide information regarding the Arrhenius parameters, such as the activation energy (E^*), the frequency factor (A), the enthalpy of activation (H^*), the entropy of activation (S^*), and the free energy of activation (G^*). Two methods were used to evaluate the kinetic thermodynamic parameters: the Coats–Redfern method [41] and the Horowitz–Metzger method [42].

3.8.1 Coats–Redfern equation

The Coats–Redfern equation (10), which is an atypical integral method, can be represented as:

$$\int_{0 \rightarrow \infty} d\alpha / (1-\alpha)^n = (A/\varphi) \int_{T_1 \rightarrow T_2} e^{-E^*/RT} dT \quad (10)$$

For convenience of integration, the lower limit T_1 is usually taken as zero. After integration, this equation can be represented as

$$\text{Ln}[-\text{Ln}(1-\alpha)/T^2] = -E^*/RT + \text{Ln}[AR/\varphi E^*] \quad (11)$$

where α is the fraction of the sample decomposed at time t , T is the derivative peak temperature, A is the frequency factor, R is the gas constant, E^* is the activation energy, and φ is the linear heating rate. A plot of the left-hand side (LHS) against $1/T$ was constructed. E^* is the energy

of activation in kJ mol^{-1} and was calculated from the slope. The A (s^{-1}) value was calculated from the intercept. The entropy of activation, ΔS^* , in ($\text{J K}^{-1} \text{mol}^{-1}$) was calculated using the equation:

$$\Delta S^* = R \ln(Ah/kT_s) \quad (12)$$

where k is the Boltzmann constant, h is Planck's constant, and T_s is the DTG peak temperature.

3.8.2 Horowitz-Metzger equation

The Horowitz-Metzger (Eg. 13) was written in the form as follows:

$$\log [\log (w_\alpha/w_\gamma)] = E^* \theta / 2.303RT_s^2 - \log 2.303 \quad (13)$$

where $\theta = T - T_s$, $w_\gamma = w_\alpha - w$, $w_\alpha =$ mass loss at the completion of the reaction; $w =$ mass loss up to time t . The plot of $\text{Log}[\log (w_\alpha/w_\gamma)]$ versus θ was drawn and found to be linear from the slope E^* was calculated. The pre-exponential factor, A , was calculated from the Eg. (14):

$$E^* \theta / RT_s^2 = A / [\varphi \exp (-E^*/RT_s)] \quad (14)$$

From the TG curves, the activation energy, E^* , entropy of activations, ΔS^* , enthalpy activations, ΔH^* , and Gibbs free energy, ΔG^* , were calculate from;

$$\Delta H^* = E^* - RT \quad \text{and} \quad \Delta G^* = \Delta H^* - T\Delta S^*$$

The evaluated kinetic parameters for the first stages based on the Coats–Redfern and Horowitz–Metzger equations are listed in Table 5. The results indicate that the kinetic data obtained from the two methods are comparable and in agreement with each other. A higher value of activation energy suggests a higher thermal stability. The [(Acf)(PA)₂] complex exhibit a higher activation energy value, which indicates the higher thermal stability of this complex. Comparing the activation energy values (E^*) of the initial decomposition for all the complex gave the order $\text{PA} > \text{TCNQ} > \text{QL} > \text{DDQ}$ for the different acceptors. The negative values of ΔS^* observed for all complexes indicate that the reaction rate is slower than normal [43]. Satisfactory values for the correlation coefficients from the Arrhenius plots of the thermal decomposition steps were observed to be $r \sim 1$ in all cases, which indicates a good fit with the linear function and reasonable agreement between the experimental data and the kinetic parameters.

Table 5. Kinetic parameters determined using the Coats-Redfern (CR) and Horowitz-Metzger (HM).

Complexes	Method	Parameters ^a				
		E^*	A	ΔS^*	ΔH^*	ΔG^*
[(Acf)(QL) ₂]	CR	2.59×10^4	5.00	-2.34×10^2	2.27×10^4	1.12×10^5
	HM	3.06×10^4	8.95×10^1	-2.10×10^2	2.74×10^4	1.08×10^5
[(Acf)(PA) ₂]	CR	7.44×10^4	4.33×10^4	-1.61×10^2	6.98×10^4	1.58×10^5
	HM	7.74×10^4	1.70×10^5	-1.50×10^2	7.28×10^4	1.55×10^5
[(Acf)(TCNQ)]	CR	6.82×10^4	6.55×10^6	-1.17×10^2	6.50×10^4	1.10×10^5
	HM	8.07×10^4	1.34×10^9	-7.24×10^1	7.75×10^4	1.05×10^5
[(Acf)(DDQ)]	CR	1.67×10^4	1.19×10^{-1}	-2.66×10^2	1.30×10^4	1.30×10^5
	HM	2.50×10^4	3.53	-2.38×10^2	2.13×10^4	1.26×10^5

3.9 XRD studies

To investigate the crystal structures of the obtained complexes, X-ray powder diffraction patterns in the range of $5^\circ < 2\theta < 60^\circ$ for the [(Acf)(QL)₂] and [(Acf)(PA)₂] complexes were examined, and the recorded patterns are shown in Fig. 10. As evident from Fig. 6, the main characteristic scattering peak of the [(Acf)(QL)₂] complex occurs at 18.504° , whereas this peak occurs at 26.350° in the diffraction pattern of the [(Acf)(PA)₂]. Based on these investigations, the sharp and well-defined Bragg peaks at specific 2θ angles confirm the semi-crystalline nature of the investigated CT complexes. The particle size of these two complexes were estimated from their XRD patterns based on the highest intensity value compared with the other peaks using the well-known Debye–Scherrer formula given in Eq. 15 [44]:

$$D = K\lambda / \beta \cos \theta \quad (15)$$

where D is the apparent particle size of the grains, K is a constant (0.94 for Cu grid), λ is the X-ray wavelength used (1.5406 Å), θ is half the scattering angle (the Bragg diffraction angle), and β is the full-width at half-maximum (FWHM) of the X-ray diffraction line (additional peak broadening) in radians. Table 6 presents the XRD spectral data for the [(Acf)(QL)₂] and [(Acf)(PA)₂] complexes, including the values of the Bragg angle (2θ), the full-width at half-maximum (β , FWHM) of the prominent intensity peak, the interplanar spacing between atoms (d), the relative intensity and the calculated particle size (D) in nm. The particle size of the complexes were estimated according to the highest value of intensity compared with the other peaks and were found to be ~ 3.2 and ~ 3.6 nm for the [(Acf)(QL)₂] and [(Acf)(PA)₂] complexes, respectively. These values confirmed that the particle sizes are located within the nanoscale range.

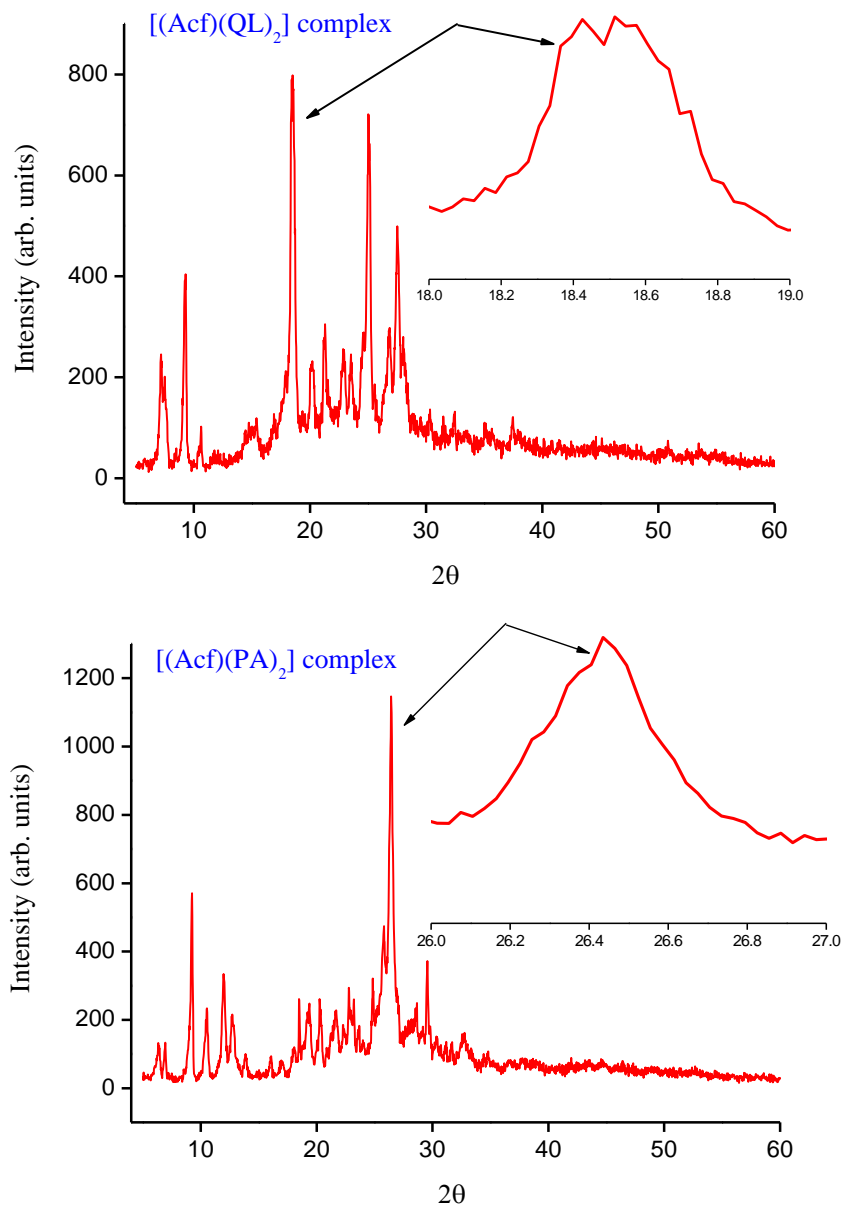


Figure 6. X-ray diffraction pattern for [(Acf)(QL)₂] and [(Acf)(PA)₂] complexes.

Table 6. XRD spectral data of [(Acf)(QL)₂] and [(Acf)(PA)₂] complexes.

Complex	2θ (°)	d value (Å)	FWHM	Relative intensity (%)	Particle size (nm)
[(Acf)(QL) ₂]	18.504	4.787	0.46	100	3.189
[(Acf)(PA) ₂]	26.350	3.368	0.43	100	3.459

3.10 SEM and EDX studies

Scanning electron microscopy (SEM) provides general information about the microstructure, the surface morphology, the particle size, the microscopic aspects of the physical behavior and the chemical composition of the respective Acf charge-transfer complexes and demonstrates the porous structures of the surface of these complexes. In addition, the chemical compositions of the complexes were determined using energy-dispersive X-ray diffraction (EDX). SEM surface images of the Acf CT complexes along with their EDX spectra are shown in Fig. 7. Analysis of the SEM images of the Acf complexes shows that the sizes of the particles are quite different with different acceptors. Furthermore, the uniformity and similarity between the particles of the synthesized Acf complexes indicate that the morphological phases of these complexes have a homogeneous matrix. Based on these observations, the [(Acf)(QL)₂], [(Acf)(TCNQ)] and [(Acf)(DDQ)] complexes particles exhibits different shapes with a particle size of ~100 μm, whereas [(Acf)(PA)₂] is semi-crystalline, and some single-phase formations exhibit well-defined shapes with a particle size of ~10 μm. In addition, the chemical compositions of the complexes were determined using energy-dispersive X-ray diffraction (EDX). The chemical analysis results from the EDX analysis for the formed complexes showed a homogeneous distribution of each acceptor. In the EDX profile, the peaks refer to all elements that constitute the molecules of these complexes; these elements were clearly identified, and the results confirmed the proposed structures.

3.11 Pharmacology

The antibacterial activity of the synthesized Acf CT complexes were tested *in vitro* against two Gram-positive bacterial strains, *Staphylococcus aureus* (*S. aureus*) and *Bacillus subtilis*, and two Gram-negative bacterial strains, *Escherichia coli* (*E. coli*) and *Pseudomonas aeruginosa* (*P. aeruginosa*). The activity was determined by measuring the inhibition zone diameter values (mm) of the complexes against the microorganisms. Tetracycline was used as a positive control. The Acf CT complexes were also screened for their antifungal properties against two fungal species, *Aspergillus flavus* and *Candida albicans*. Amphotericin B was used as a positive control. The screening data are reported in Table 7 and are statistically presented in Fig. 8. The results indicated that the Acf complexes showed varying degrees of inhibition against the all tested microorganisms. In general, the best antibacterial and antifungal activity were displayed by [(Acf)(QL)₂] complex. Regarding the inhibition zone diameter, [(Acf)(QL)₂] complex had the highest antimicrobial activity against the growth of the tested organisms compared to other tested complexes. It gained approximately 58% of activity of antibacterial agent (Tetracycline) and 76% of the activity of antifungal agent (Amphotericin B). The data also reveal that [(Acf)(QL)₂] is the only complex that showed good inhibitory activity against the growth of the tested fungal strains. [(Acf)(PA)₂] display moderately activity against *Candida albicans*, whereas [(Acf)(TCNQ)] and [(Acf)(DDQ)] complexes exhibited no inhibitory activity against either fungal species. The [(Acf)(PA)₂], [(Acf)(TCNQ)] and [(Acf)(DDQ)] complexes exhibited moderate inhibitory results against all of the Gram-positive and Gram-negative bacterial species, as reported in Table 7. The marked activity of [(Acf)(QL)₂]

complex may be due to the outer membrane of all target organisms (bacteria or fungus) more permeable for [(Acf)(QL)₂] complex than other complexes. The most reasons for lethal action of tested complexes may due to their interactions with critical intercellular sites causing the death of cells. The variety of antimicrobial activities of tested complexes may due to a different degree of tested complexes penetration through cell membrane structure of target organism [45].

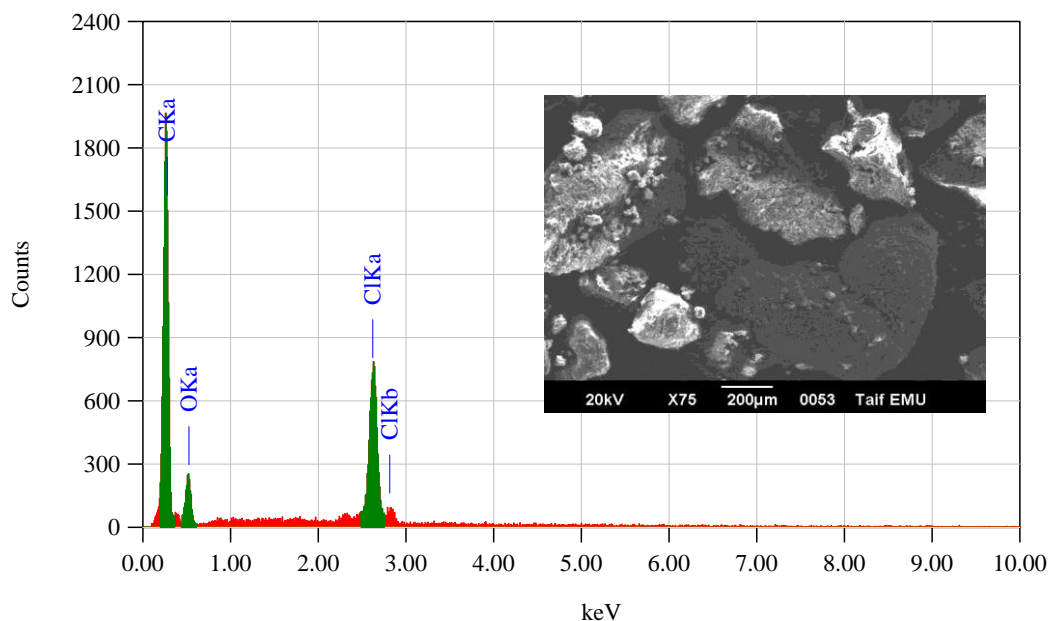


Figure 7A. SEM images and EDX spectrum of [(Acf)(QL)₂] complex.

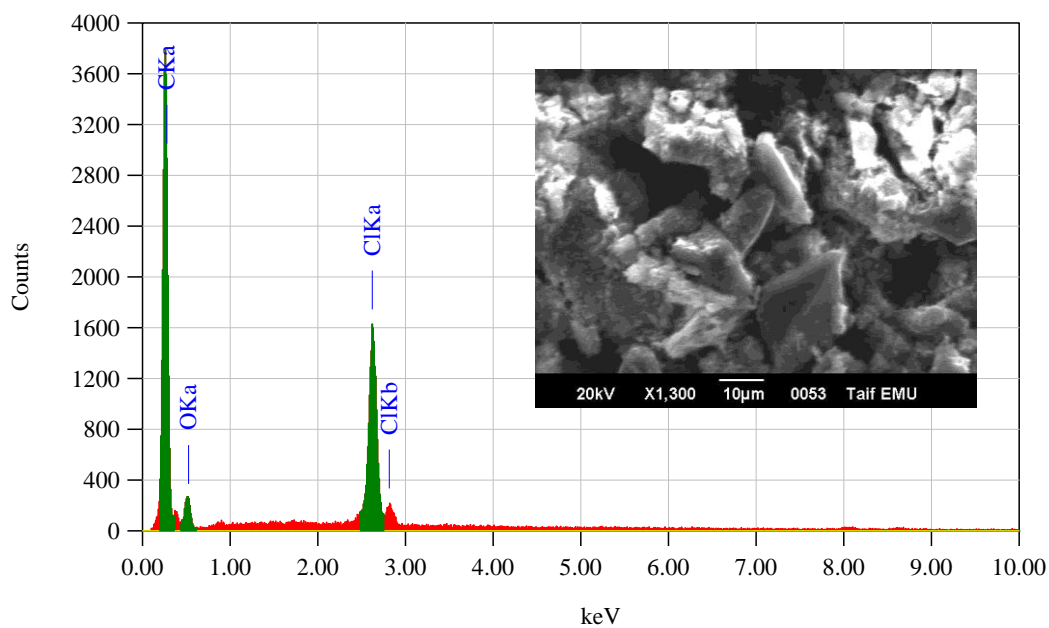


Figure 7B. SEM images and EDX spectrum of [(Acf)(PA)₂] complex.

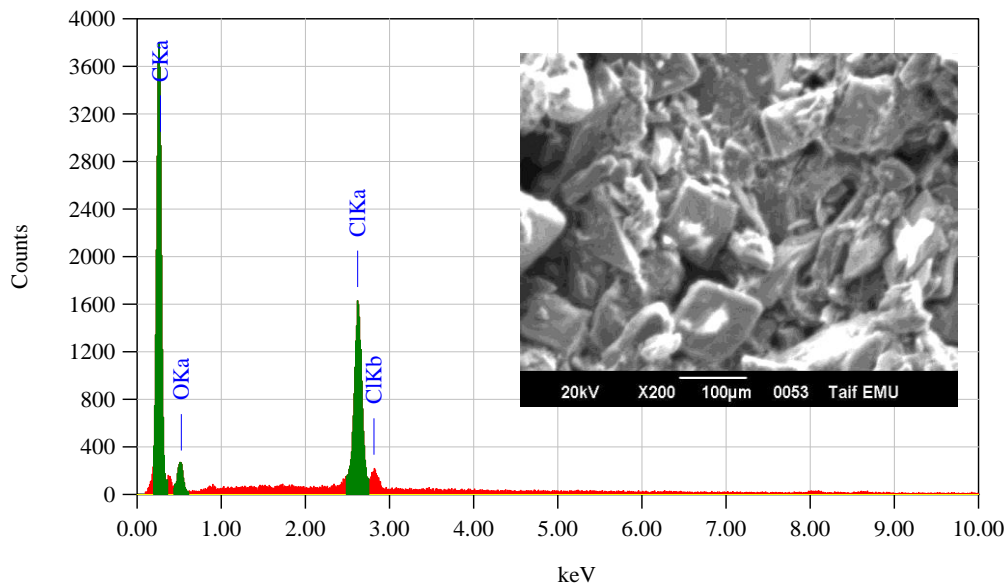


Figure 7C. SEM images and EDX spectrum of [(Acf)(TCNQ)] complex.

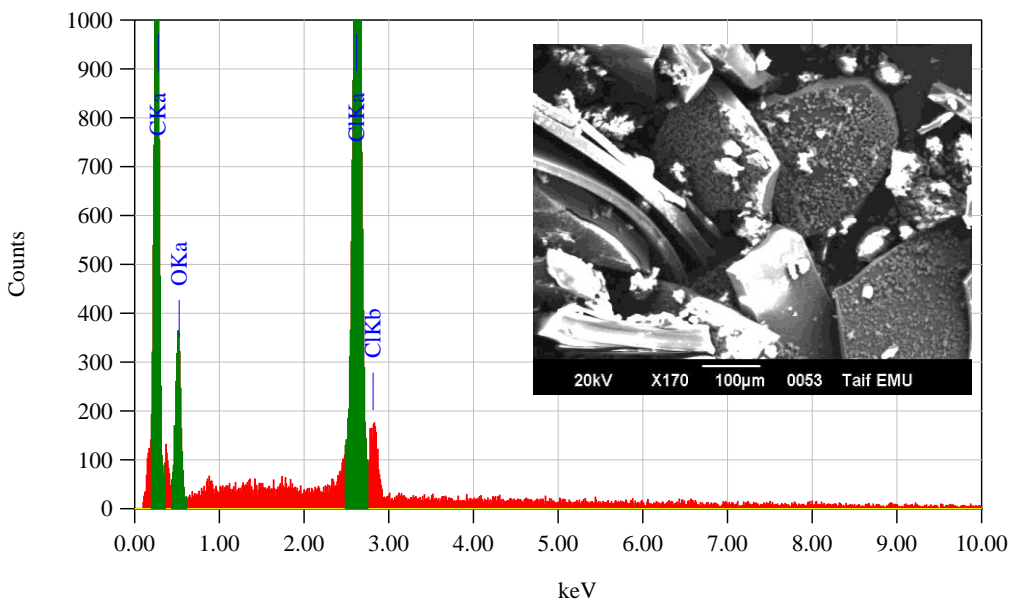


Figure 7D. SEM images and EDX spectrum of [(Acf)(DDQ)] complex.

Table 7. The inhibition diameter zone values (mm) for Acf CT-complexes.

Sample	Inhibition zone diameter (mm/mg sample)					
	Bacteria				Fungi	
	<i>Bacillus subtilis</i> , (G ⁺) ^a	<i>Escherichia coli</i> , (G ⁻)	<i>Pseudomonas aeruginosa</i> , (G ⁻)	<i>Staphylococcus aureus</i> , (G ⁺)	<i>Aspergillus flavus</i>	<i>Candida albicans</i>
Control: DMSO	0.0	0.0	0.0	0.0	0.0	0.0
Tetracycline	34.0	32.0	34.0	30.0	-	-
Amphotericin B	-	-	-	-	18.0	19.0
Acf/QL	20.0	20.0	17.0	22.0	12.0	17.0
Acf/PA	14.0	15.0	14.0	16.0	0.0	12.0
Acf/TCNQ	10.0	13.0	10.0	0.0	0.0	0.0
Acf/DDQ	14.0	15.0	16.0	16.0	0.0	0.0

^a G: Gram reaction.

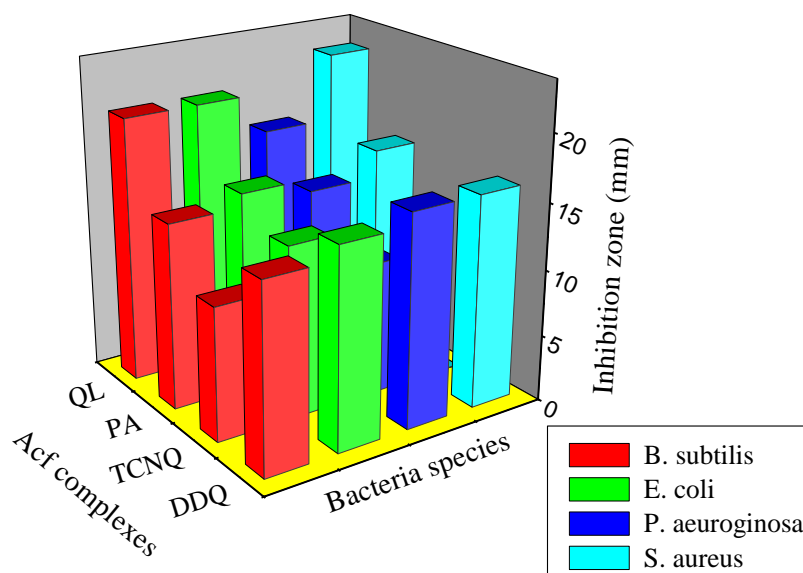


Figure 8A. Statistical representation for antibacterial activity of Acf complexes.

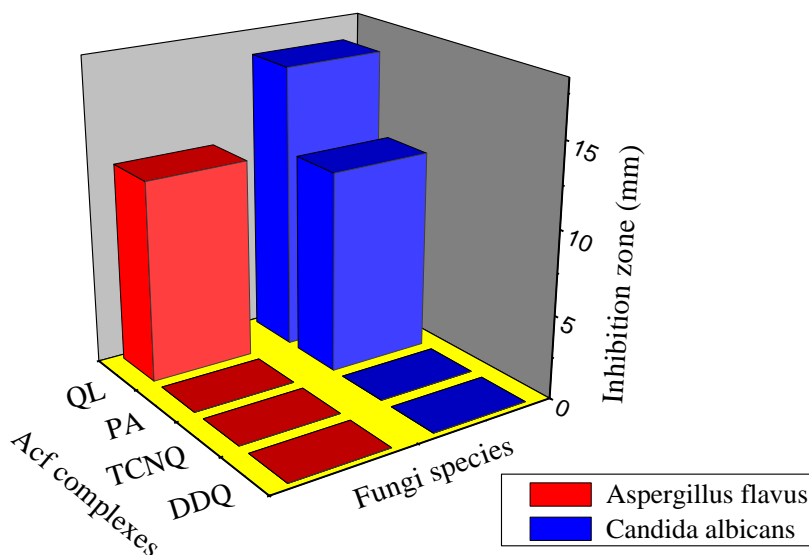


Figure 8B. Statistical representation for antifungal activity of Acf complexes.

References

1. J. Martínez Calatayud, R.M. Villanueva Camañas, *Quím. Anal.* 4 (1985) 91.
2. R.M. Acheson (Ed.), *Aromatic Heterocyclic Compounds: The Acridine*, Interscience, New York, 1973.
3. Po-Chin Nien, Po-Yen Chen, Kuo-Chuan Ho, *Sensors and Actuators B* 140 (2009) 58.
4. M. Wainwright, *J. Antimicrob. Chemother.* 47 (2001) 1.
5. Y. Li, H. Kuwabara, Y.K. Gong, Y. Takaki, K. Nakashima, *J. Photochem. Photobiol. B* 70 (2003) 171.
6. M. Shamsipur, M.J. Chaichi, A.R. Karami, *Spectrochim. Acta A* 59 (2003) 511.
7. J.M. Calatayud, J.V.G. Mateo, V. David, *Analyst* 123 (1998) 429.

8. Y.Q. Zi, L.G. Chen, J. Chen, *Chin. J. Anal. Chem.* 27 (1999) 691.
9. O.R. Pons, D.M. Gregorio, J.V. García Mateo, J.M. Calatayud, *Analytica Chimica Acta* 438 (2001) 149.
10. D.A. Skoog, *Principle of Instrumental Analysis*, third ed., Saunders, New York, USA, 1985 (Chapter 7).
11. H.A. Benesi, J.H. Hildebrand, *J. Am. Chem. Soc.* 71 (1949) 2703.
12. R. Abu-Eittah, F. Al-Sugeir, *Can. J. Chem.* 54 (1976) 3705.
13. A.W. Bauer, W.M. Kirby, C. Sherris, M. Turck, *Am. J. Clin. Pathol.* 45 (1966) 493.
14. M.A. Pfaller, L. Burmeister, M.A. Bartlett, M.G. Rinaldi, *J. Clin. Microbiol.* 26 (1988) 1437.
15. D.J. Beecher, A.C. Wong, *Appl. and Environ. Microbiol.* 60 (1994) 1646.
16. National Committee for Clinical Laboratory Standards. *Methods for Antimicrobial Susceptibility Testing of Anaerobic Bacteria: Approved Standard M11- A3*. NCCLS, Wayne, PA, USA (1993).
17. National Committee for Clinical Laboratory Standards. *Reference Method for Broth Dilution Antifungal Susceptibility Testing of Conidium-Forming Filamentous Fungi: Proposed Standard M38-A*. NCCLS, Wayne, PA, USA (2002).
18. National Committee for Clinical Laboratory Standards. *Method for Antifungal Disk Diffusion Susceptibility Testing of Yeast: Proposed Guideline M44-P*. NCCLS, Wayne, PA, USA (2003).
19. H. Tsubomura, R.P. Lang, *J. Am. Chem. Soc.* 83 (1961) 2085.
20. R. Rathone, S.V. Lindeman, J.K. Kochi, *J. Am. Chem. Soc.* 119 (1997).
21. G. Aloisi, S. Pignataro, *J. Chem. Soc. Faraday Trans.* 69 (1972) 534.
22. G. Briegleb, J. Czekalla, *Z. Physikchem, Frankfurt* 24 (1960) 237.
23. G. Briegleb, *Z. Angew. Chem.* 72 (1960) 401, *Z. Angew. Chem.* 76 (1964) 326.
24. A.N. Martin, J. Swarbrick, A. Cammarata, *Physical Pharmacy*, 3rd ed., Lee and Febiger, Philadelphia, PA, 1969, p. 344.
25. M.S. Refat, A. Elfalaky, E. Elesh, *J. Mol. Struct.* 990 (2011) 217.
26. M. Pandeewaran, K.P. Elango, *Spectrochim. Acta A* 65 (2006) 1148.
27. J. Swaminathan, M. Ramalingam, V. Sethuraman, N. Sundaraganesan, S. Sebastian, *Spectrochim. Acta A* 73 (2009) 593.
28. M.S. Refat, L.A. El-Zayat, O.Z. Yesilel, *Spectrochim. Acta A* 75 (2010) 745.
29. M.S. Refat, H.A. Saad, A.A. Adam, *J. Mol. Struct.* 995 (2011) 116.
30. L.J. Bellamy, *The infrared Spectra of Complex Molecules*, Chapman & Hall, London, 1975.
31. R. Bharathikannan, A. Chandramohan, M.A. Kandhaswamy, J. Chandrasekaran, R. Renganathan, V. Kandavelu, *Cryst. Res. Technol.* 43 (6) (2008) 683.
32. A.S. Gaballa, S.M. Teleb, E. Nour, *J. Mol. Struct.* 1024 (2012) 32.
33. A.A. Adam., M.S. Refat, T. Sharshar, Z.K. Heiba, *Spectrochim. Acta A* 95 (2012) 458.
34. A.A. Adam, *J. Mol. Struct.* 1030 (2012) 26.
35. R.D. Kross, V.A. Fassel, *J. Am. Chem. Soc.* 79 (1957) 38.
36. M.S. Refat, *J. Mol. Struct.* 985 (2011) 380.
37. G.G. Mohamed, Shaban M. Khalil, M.A. Zayed, M. Abd El-Hamid El-Shall, *J. Pharm. Biomed. analysis* 28 (2002) 1127.
38. A.S. Amine, M.E. Moustafa, Y.M. Issa, *Microchem. J.* 50 (1994) 6.
39. N. Singh, A. Ahmad, *J. Mol. Struct.* 977 (2010) 197.
40. R.D. Kross, V.A. Fassel, *J. Am. Chem. Soc.* 79 (1957) 38.
41. A.W. Coats, J.P. Redfern, *Nature (London)* 201 (1964) 68.
42. H.H. Horowitz, G. Metzger, *Anal. Chem.* 35 (1963) 1464.
43. A.A. Frost, R.G. Pearson, *Kinetics and Mechanism*, Wiley, New York, NY, USA, 1961.
44. S.J.S. Qazi, A.R. Rennie, J.K. Cockcroft, M. Vickers, *J. Colloid Interface Sci.* 338 (2009) 105.
45. A.A. El-Habeeb, F.A. Al-Saif, M.S. Refat, *J. Mol. Struct.* 1034 (2013) 1.